Continuous generation and stabilization of mesoscopic field superposition states in a quantum circuit

Ananda Roy,[1,2,3,*] Zaki Leghtas,[1] A. Douglas Stone,[1] Michel Devoret,[1] and Mazyar Mirrahimi[3,1]

[1]*Department of Applied Physics, Yale University, P.O. Box 208284, New Haven, Connecticut 06511, USA*

[2]*Laboratoire Pierre Aigrain, Ecole Normale Suprieure, CNRS (UMR 8551), Universit Pierre et Marie Curie, Universit D. Diderot 24, rue Lhomond, 75231 Paris Cedex 05, France*

[3]*INRIA Paris-Rocquencourt, Domaine de Voluceau, B.P. 105, 78153 Le Chesnay Cedex, France*

(Received 7 November 2014; published 7 January 2015)

While dissipation is widely considered to be harmful for quantum coherence, it can, when properly engineered, lead to the stabilization of nontrivial pure quantum states. We propose a scheme for continuous generation and stabilization of Schrödinger cat states in a cavity using dissipation engineering. We first generate nonclassical photon states with definite parity by means of a two-photon drive and dissipation, and then stabilize these transient states against single-photon decay. The single-photon stabilization is autonomous, and is implemented through a second engineered bath, which exploits the photon-number-dependent frequency splitting due to Kerr interactions in the strongly dispersive regime of circuit QED. Starting with the Hamiltonian of the baths plus cavity, we derive an effective model of only the cavity photon states along with analytic expressions for relevant physical quantities, such as the stabilization rate. The deterministic generation of such cat states is one of the key ingredients in performing universal quantum computation.

DOI: 10.1103/PhysRevA.91.013810 PACS number(s): 42.50.Dv, 03.65.Yz, 03.67.Lx, 42.50.Pq

I. INTRODUCTION

Quantum computing has shown great promise as a resource providing exponential speedup over certain classical algorithms and as an indispensable tool for efficient simulation of quantum systems [1–4]. Recent years have seen considerable effort in understanding how a quantum computer outperforms its classical counterpart. An essential ingredient has been identified for systems performing universal quantum computation with continuous variables (e.g., modes of electromagnetic field), namely, nonclassical states, i.e., states displaying negativity in their Wigner function [5–9]. This can be achieved by engineering a Hamiltonian with terms higher than quadratic in mode amplitude, for instance, the Kerr Hamiltonian, which is quartic [10]. Such a Hamiltonian, together with linear scattering elements such as beam splitters, drives, and squeezers, is sufficient to perform arbitrary polynomial transformations of the mode variables [11].

Nonclassical input states such as single photons and superpositions of coherent states are the main candidates for universal quantum computation with linear optical circuits [12–15]. This has stimulated experiments in which single-photon states are generated in a heralded [16–18] and on-demand [19,20] manner. Various experimental schemes have likewise produced and observed superposition of coherent states in optical systems in a heralded manner using photon subtraction [21–25]. In the context of cavity or circuit QED, such superposition states have been generated by mapping a qubit state to a coherent-state superposition in a heralded manner [26] and on demand [27]. Here, we go a step further and address the question of robustly stabilizing cavity photons in a superposition of coherent states. This could act as a continuous and deterministic source of nonclassical input states in quantum information processing protocols.

To that end, we apply a dissipation engineering technique leading to an autonomous preparation and protection against decoherence of these states [28]. An earlier theoretical proposal within the framework of cavity QED with Rydberg atoms describes such a stabilization by an adequate engineered system-bath interaction [29]. The current proposal is adapted to photon states in quantum superconducting circuits, and requires only the application of continuous-wave (CW) microwave drives of fixed frequencies and amplitudes, thus greatly simplifying an experimental implementation.

The first stage of our proposal builds on recent theoretical work in such systems [30] in which a bath was engineered such that photons are only exchanged in pairs. Such a nonlinear system-bath interaction was shown to stabilize the manifold spanned by two coherent states $|\alpha\rangle$ and $|-\alpha\rangle$ (where α, the coherent-state amplitude parameter, is determined by a tunable external drive). Very recently, this proposal has been implemented successfully in an experimental setup [31]. The dynamics generated by such an interaction conserves photon-number parity: an initial vacuum state $|0\rangle$ would therefore converge to the even Schrödinger cat state $|C_\alpha^+\rangle = \sum_{n=0}^{\infty} c_{2n}|2n\rangle$, $c_m = \frac{e^{-|\alpha|^2/2}}{\sqrt{2(1+e^{-2|\alpha|^2})}}\frac{\alpha^m}{\sqrt{m!}}$. Similarly, an odd-parity initial state will converge to the odd Schrödinger cat state $|C_\alpha^-\rangle = \sum_{n=0}^{\infty} c_{2n+1}|2n+1\rangle$. Finally, an initial state with undefined parity will converge to a final state of undefined parity. In practice, however, while one can add a two-photon bath interaction which transiently dominates the dynamics, there will always be a residual single-photon loss channel that will decohere these parity superpositions, leading to a statistical mixture of $|\alpha\rangle$ and $|-\alpha\rangle$ in the steady state.[1]

In this paper, we present a theoretical proposal where we autonomously compensate for single-photon loss and

*ananda.roy@yale.edu

[1]The changes in photon-number parity resulting from single-photon loss can, in principle, be continuously monitored [32] and compensated for, in a measurement-based feedback scheme.

ensure the stabilization of a single superposition [e.g., $|C_\alpha^+\rangle = \frac{1}{\sqrt{2(1+e^{-2|\alpha|^2})}}(|\alpha\rangle + |-\alpha\rangle)$] in this manifold. Similarly to some recent autonomous stabilization protocols for superconducting qubits [33–35], we benefit from the high-quality factors of the superconducting microwave resonators in the presence of strong nonlinear interactions provided by Josephson elements. More precisely, we make use of the dispersive (cross-Kerr) interaction between two cavity modes mediated by a transmon qubit coupled to both of them [36]. Working in the strong dispersive regime [37], we design an effective decay of the cavity mode from a cat state of odd parity to a cat state of even parity. This dissipation, together with the two-photon process, reduces the steady state from a manifold spanned by $\{|C_\alpha^+\rangle, |C_\alpha^-\rangle\}$ to a unique state ($|C_\alpha^+\rangle$). The full system requires only a high-Q "storage cavity," coupled to two low-Q "readout cavities" through Josephson junctions and requires cavity decay and coupling parameters well within the reach of current technology. A trivial modification of the scheme leads to stabilization of $|C_\alpha^-\rangle$. Note that even though we use the term "readout" to refer to the dissipative baths, the information leaking through the ports associated with the two low-Q cavities does not need to be monitored. It suffices that it never returns to the stabilized "storage cavity."

The paper is organized as follows: in Sec. II, we describe our dissipation engineering scheme that stabilizes an even Schrödinger cat state. In Sec. III, we describe the possible experimental implementation, engineering the Hamiltonian interactions and dissipation, that realizes the stabilization scheme. We sweep the parameters that are, in principle, tunable in an ongoing experiment to determine the optimal choice. Next, we perform adiabatic elimination of the faster dynamical variables to arrive at an effective interaction and dissipation for the storage cavity alone, providing analytic expressions for the various decay and interaction rates (Sec. III C). We summarize our results in Sec. IV.

II. TWO-PHOTON PROCESS AND PARITY SELECTION

In this section, we briefly outline the interaction and dissipation scheme that gives rise to an even Schrödinger cat state ($|C_\alpha^+\rangle$) in the steady-state regime. We assume, for the storage cavity, the existence of a single-photon decay channel which is the natural dominant decoherence channel in the absence of engineered system-bath interactions. We further assume that we have engineered two additional decay channels: the two-photon decay channel through which pairs of photons are lost into the environment (following previous work [30,38–41]), and a parity-selection decay channel, which leads to an effective transfer of population from the odd to the even photon-number parity manifold. These decay channels are characterized by effective decay rates $\kappa_{2\mathrm{ph}}$ and κ_{ps}, respectively, and we assume that we can engineer them to be much larger than the rate of single-photon loss ($\kappa_{1\mathrm{ph}}$) for the relevant cavity modes:

$$\kappa_{1\mathrm{ph}} \ll \kappa_{2\mathrm{ph}}, \kappa_{\mathrm{ps}}. \tag{1}$$

A. Two-photon process

Consider a cavity mode coupled to a bath and a drive such that it absorbs or loses photons only in pairs. Denoting the annihilation operator for this two-photon driven-dissipative harmonic oscillator as $\mathbf{a_s}$, the master equation for the mode is

$$\frac{d\rho}{dt} = -i[\mathbf{H}_{2\mathrm{ph}}, \rho] + \kappa_{2\mathrm{ph}}\mathcal{D}\left(\mathbf{a_s}^2\right)\rho + \kappa_{1\mathrm{ph}}\mathcal{D}(\mathbf{a_s})\rho, \tag{2}$$

where $\mathcal{D}(\hat{O})\rho = \hat{O}\rho\hat{O}^\dagger - \frac{1}{2}\hat{O}^\dagger\hat{O}\rho - \frac{1}{2}\rho\hat{O}^\dagger\hat{O}$ is the usual Lindblad operator, $\mathbf{H}_{2\mathrm{ph}} = i(\epsilon_{2\mathrm{ph}}\mathbf{a_s}^{\dagger 2} - \epsilon_{2\mathrm{ph}}^*\mathbf{a_s}^2)$, and $\epsilon_{2\mathrm{ph}}$ is the two-photon drive strength. As noted, for $\kappa_{1\mathrm{ph}} = 0$, one can show that starting from vacuum [$\rho(t=0) = |0\rangle\langle 0|$], the density matrix converges towards $\rho(t\to\infty) = |C_\alpha^+\rangle\langle C_\alpha^+|$, where $\alpha = \sqrt{2\epsilon_{2\mathrm{ph}}/\kappa_{2\mathrm{ph}}}$ [30]. In the presence of single-photon loss, due to the random photon jumps, the cat state undergoes decoherence resulting in an incoherent mixture of $|\alpha\rangle$ and $|-\alpha\rangle$.

B. Parity selection

In order to compensate for the decoherence due to single-photon loss, we consider the action of effective jump operators of the form $\mathbf{J}_{2n} = |2n\rangle\langle 2n+1|$, which acting on the odd-number states bring it to the immediate lower even-number state. This transfers the excitations from the odd-parity manifold, which gets populated due to single-photon loss, to the even-parity manifold. Once the population is transferred to the even manifold, the two-photon process redistributes the population over the even manifold so as to reach the steady state determined by the two-photon bath plus drive, $|C_\alpha^+\rangle$. Let us consider, for simplicity, only one such operator: $\mathbf{J}_{2\tilde{n}} = |2\tilde{n}\rangle\langle 2\tilde{n}+1|$, where $2\tilde{n}$ is the even integer closest to the average number of photons in the even cat $|C_\alpha^+\rangle$.[2] The two-photon process acts also on the odd manifold, where it redistributes population, with maximum around $|2\tilde{n}+1\rangle$, so as to funnel probability density towards the escape channel given by the jump operator, $\mathbf{J}_{2\tilde{n}}$. Thus, although by itself this jump operator only transfers the population from the Fock state $|2\tilde{n}+1\rangle$ to $|2\tilde{n}\rangle$, together with the two-photon process, it drains the population from the odd to the even manifold (cf. Fig. 1). The rate associated with this parity-selection process will be denoted by κ_{ps}. Thus, we can write the master equation governing the stabilized evolution of the cavity mode,

$$\frac{d\rho}{dt} = -i[\mathbf{H}_{2\mathrm{ph}}, \rho] + \kappa_{2\mathrm{ph}}\mathcal{D}\left(\mathbf{a_s}^2\right)\rho + \kappa_{1\mathrm{ph}}\mathcal{D}(\mathbf{a_s})\rho + \kappa_{\mathrm{ps}}\mathcal{D}(\mathbf{J}_{2\tilde{n}})\rho. \tag{3}$$

In Fig. 2, we show the results of simulation of this equation. On the right is shown the Wigner function for the final state for $\alpha = 2$ when all terms are present in the evolution equation. The interference fringes near the origin clearly show the negativity of the Wigner function. On the left, we show the time evolution of the fidelity of the solution of the evolution equation with respect to the ideal target state for three cases. In the absence of single-photon loss ($\kappa_{1\mathrm{ph}} = 0$), the fidelity approaches unity at a

[2] If the desired target state is $|C_\alpha^-\rangle$, one needs to consider jump operators of the form $\mathbf{J}_{2\tilde{n}-1} = |2\tilde{n}-1\rangle\langle 2\tilde{n}|$.

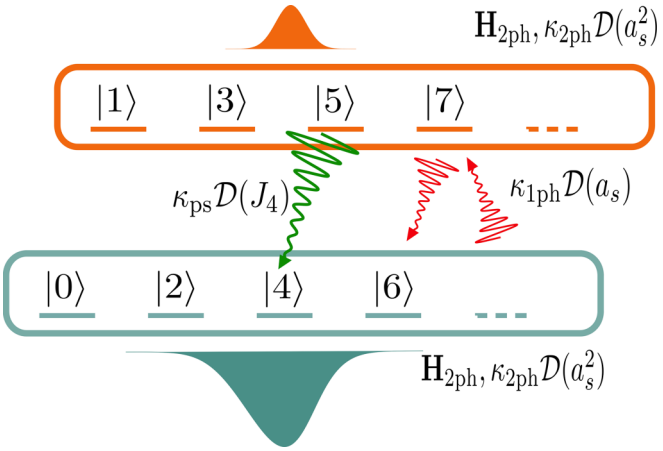

FIG. 1. (Color online) Schematic for the stabilization of the "cat state," $|C^+_{\alpha=2}\rangle$. The two-photon drive and dissipation [denoted by $\mathbf{H}_{2\mathrm{ph}}, \kappa_{2\mathrm{ph}}\mathcal{D}(a_s^2)$] act on the even and odd manifolds, shown in blue and orange, respectively. In the absence of single-photon loss and starting from vacuum, the odd manifold remains unpopulated, while the even manifold population is distributed to realize an even cat state. However, single-photon loss (shown in red) denoted by $\kappa_{1\mathrm{ph}}\mathcal{D}(a_s)$ transfers some of the population to the odd manifold, where it is distributed as in an odd cat state due to the two-photon drive and/or dissipation. We propose to engineer a dissipation interaction from $|5\rangle$ to $|4\rangle$ (in green) denoted by $\kappa_{\mathrm{ps}}\mathcal{D}(J_4)$. This dissipation, together with the two-photon process, transfers excitations from the odd to even manifold and stabilizes the desired cat state.

rate determined by $\kappa_{2\mathrm{ph}}$. When single-photon loss is added, but not stabilization ($\kappa_{1\mathrm{ph}} \neq 0, \kappa_{\mathrm{ps}} = 0$), the fidelity grows initially but then decays to 0.5 as expected for the statistical mixture (asymptotic behavior data not shown here). When all three processes are present, the fidelity stabilizes at a value greater than 0.9. (For fidelity of a density matrix ρ with respect to the target state $|C^+_\alpha\rangle$, we use the definition $F = \langle C^+_\alpha|\rho|C^+_\alpha\rangle$.)

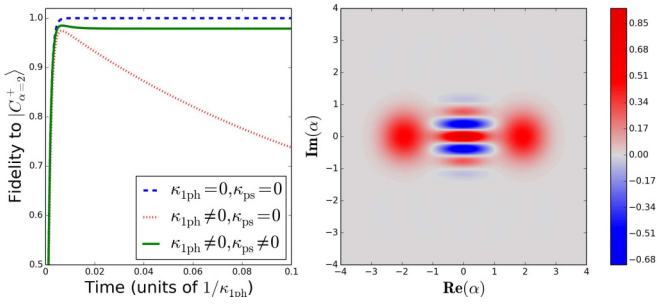

FIG. 2. (Color online) Fidelity with respect to the target state $|C^+_{\alpha=2}\rangle$ (left panel) and Wigner function of the steady state (right panel). The parity-selecting dissipation and the two-photon dissipation and/or drive, in the presence of single-photon loss, stabilizes the even cat state. The dissipation rates are $\kappa_{2\mathrm{ph}} = 250\kappa_{1\mathrm{ph}}, \kappa_{\mathrm{ps}} = 760\kappa_{1\mathrm{ph}}$. The evolution of fidelity is shown in the absence of single-photon loss (blue dashed line), in the presence of single-photon loss and the absence of parity selection (red double-dashed line), and, lastly, in the presence of single-photon loss and parity selection (green solid line). The steady-state Wigner function of the stabilized cat state is shown in the presence of single- and two-photon loss and parity selection.

Here we choose the two-photon dissipation rate and the parity-selection rate to be $\kappa_{2\mathrm{ph}} = 250\kappa_{1\mathrm{ph}}, \kappa_{\mathrm{ps}} = 760\kappa_{1\mathrm{ph}}$, consistent with the required inequality (1) above.

The master equation we have studied is an idealized "cavity-only" system, whereas additional components will be required to realize the required baths and drives. In the following section, we propose a possible experimental implementation of the aforementioned stabilization scheme. Subsequently, we will analyze the reduction of this system to an effective model described by the single-cavity master equation.

III. PROPOSED EXPERIMENTAL IMPLEMENTATION

We propose a three-cavity two-junction architecture, where a high-Q cavity (referred to as storage cavity s) is linked by small transmission lines to two low-Q cavities, referred to as readout cavities r_1 and r_2, as shown in Fig. 3. Each transmission line has an in-line embedded Josephson junction, which by virtue of the Josephson nonlinearity provides a nonlinear coupling between the storage and readout cavities. The single-photon loss rate of the storage cavity is given by $\kappa_{1\mathrm{ph}}$, while that of the two readout cavities are given by κ_{r_1} and κ_{r_2} with the constraint

$$\kappa_{1\mathrm{ph}} \ll \kappa_{r_1}, \kappa_{r_2}. \tag{4}$$

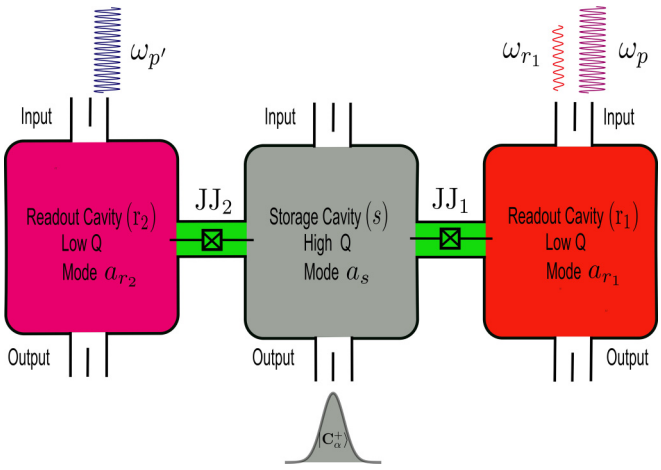

FIG. 3. (Color online) Schematic of experimental setup realizing the stabilization scheme. Josephson junction JJ_1 bridges the storage and readout cavity r_1. This, together with the stiff off-resonant pump at $\omega_p = 2\omega_s - \omega_{r_1}$, and the weak resonant drive at ω_{r_1} incident on r_1, gives rise to the two-photon drive and dissipation. Josephson junction JJ_2 bridges the storage and readout cavity r_2 providing a nonlinear coupling between the modes $\mathbf{a_s}$ and low-Q mode $\mathbf{a_{r_2}}$. An off-resonant pump incident on r_2 at frequency $\omega_{p'} = (\omega_{r_2} - \omega_s - 2\tilde{n}\chi_{sr_2})/2$ gives rise to beam-splitter-like interaction between $\mathbf{a_s}$ and $\mathbf{a_{r_2}}$: $g_{\mathrm{ps}}e^{2i\omega_{p'}t}\mathbf{a_s}^\dagger\mathbf{a_{r_2}} + \mathrm{c.c.}$ This beam-splitter-like interaction acts conditioned on the mode $\mathbf{a_s}$ having $2\tilde{n}+1$ photons in the storage cavity. When the condition is realized, this interaction transfers one quantum of excitation from the $\mathbf{a_s}$ mode to the $\mathbf{a_{r_2}}$ mode, which is then lost irreversibly to the environment.

The Hamiltonian of this device can be written as [42]

$$\mathbf{H}_0 = \sum_k \hbar\omega_k \mathbf{a}_k^\dagger \mathbf{a}_k - E_{J_1}\left[\cos\left(\frac{\Phi_1}{\phi_0}\right) + \frac{1}{2}\left(\frac{\Phi_1}{\phi_0}\right)^2\right] - E_{J_2}\left[\cos\left(\frac{\Phi_2}{\phi_0}\right) + \frac{1}{2}\left(\frac{\Phi_2}{\phi_0}\right)^2\right]. \quad (5)$$

Here, $E_{J_{1,2}}$ are the Josephson energy for the two junctions, ω_k are the bare frequencies of the modes $\mathbf{a}_k$, $\phi_0 = \hbar/2e$ is the reduced flux quantum, and $\Phi_{1,2}$ is the flux through the Josephson junction linking readout cavity $r_{1,2}$ to storage cavity s.

Here, only the fundamental modes of the three cavities are excited, annihilation operators (frequencies) of which are denoted, respectively, by $\mathbf{a_s}(\omega_s)$,$\mathbf{a_{r_1}}(\omega_{r_1})$, and $\mathbf{a_{r_2}}(\omega_{r_2})$. The Josephson junctions ensure a nonlinear coupling of the modes $\mathbf{a_s}$ and $\mathbf{a_{r_1}}$, and similarly between the modes $\mathbf{a_s}$ and $\mathbf{a_{r_2}}$. This gives rise to self-Kerr and cross-Kerr interactions of the form $-\frac{\chi_{ff}}{2}\mathbf{f}^{\dagger 2}\mathbf{f}^2$ and $-\chi_{fg}(\mathbf{f}^\dagger\mathbf{f})(\mathbf{g}^\dagger\mathbf{g})$, where $\mathbf{f},\mathbf{g}$ correspond to the annihilation operators for the modes under consideration. Our stabilization scheme makes use of the following separation of time scales (cf. Secs. III A and III B for details):

$$\chi_{sr_1} \ll \kappa_{r_1} \text{ and } \kappa_{r_2} \ll \chi_{sr_2}. \quad (6)$$

This separation of time scales can be engineered by appropriately choosing the participation ratios of the modes interacting through the junction nonlinearity.

A. Realizing two-photon process

We can engineer a nonlinear interaction between the two modes $\mathbf{a_s}$ and $\mathbf{a_{r_1}}$ by means of a stiff (nondepleted), off-resonant pump incident on the readout cavity r_1. The frequency ω_p of the pump is chosen to be $\omega_p = 2\omega_s - \omega_{r_1}$. In addition, we drive the mode $\mathbf{a_{r_1}}$ with a weak *resonant* tone of amplitude ϵ_{r_1} and frequency ω_{r_1}. Following the same kind of analysis as in [42] and setting $\hbar = 1$ for the rest of this work, one can write the effective interaction Hamiltonian between the modes $\mathbf{a_s}$ and $\mathbf{a_{r_1}}$ as (see Fig. 4)

$$\mathbf{H}_{sr_1} = \omega_s \mathbf{a_s}^\dagger \mathbf{a_s} + \omega_{r_1} \mathbf{a_{r_1}}^\dagger \mathbf{a_{r_1}} + g_{2\text{ph}}\left(\mathbf{a_s}^{\dagger 2}\mathbf{a_{r_1}} + \mathbf{a_s}^2 \mathbf{a_{r_1}}^\dagger\right) - \epsilon_{r_1}\left(\mathbf{a_{r_1}} + \mathbf{a_{r_1}}^\dagger\right) - \frac{\chi_{ss}}{2}\mathbf{a_s}^{\dagger 2}\mathbf{a_s}^2 - \frac{\chi_{r_1 r_1}}{2}\mathbf{a_{r_1}}^{\dagger 2}\mathbf{a_{r_1}}^2 - \chi_{sr_1}(\mathbf{a_s}^\dagger \mathbf{a_s})\left(\mathbf{a_{r_1}}^\dagger \mathbf{a_{r_1}}\right), \quad (7)$$

where we have assumed the nonlinear coupling $g_{2\text{ph}}$ and drive amplitude ϵ_{r_1} to be real (phase of $g_{2\text{ph}}$ is fixed by the phase of the stiff pump at ω_p) and neglected nonlinearity higher than fourth order in mode amplitudes. In writing Eq. (7), we have also included self-Kerr and cross-Kerr interaction terms of the modes $\mathbf{a_s}$,$\mathbf{a_{r_1}}$ arising out of $\mathbf{H}_0$. As shown in [30],

$$g_{2\text{ph}} = \frac{\epsilon_p}{\omega_p - \omega_{r_1}}\chi_{sr_1}/2, \quad (8)$$

where ϵ_p is the amplitude of the pump drive. For the rate inequalities given by Eq. (6), the Hamiltonian [Eq. (7)], together with the decay of the low-Q mode $\mathbf{a_{r_1}}$, gives rise to the two-photon drive and dissipation of Eq. (2) (cf. [31] and chapter 12 of [43] for details of the calculation).

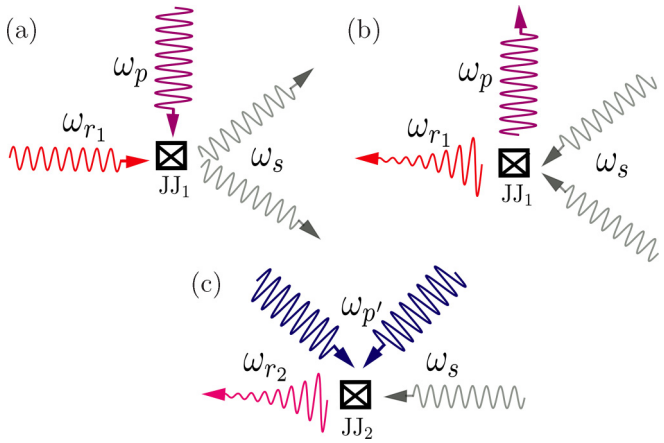

FIG. 4. (Color online) Scattering processes taking place through the nonlinear elements. (a) One photon in readout mode $\mathbf{a_{r_1}}$, together with one photon of pump at ω_p, gets converted to two photons in mode $\mathbf{a_s}$, giving rise to the two-photon drive. (b) Two photons of the mode $\mathbf{a_s}$ are converted into one photon in pump mode at frequency ω_p and one photon in mode $\mathbf{a_{r_1}}$, which then irreversibly decays to the environment, giving rise to two-photon dissipation. (c) One photon in the mode $\mathbf{a_s}$, along with two photons in the pump with the adequate frequency $\omega_{p'}$, are converted conditionally into a photon in mode $\mathbf{a_{r_2}}$, which then irreversibly decays to the environment. This process occurs only when the number of photons in the storage cavity is $2\tilde{n}+1$, giving rise to the parity-selection mechanism.

B. Realizing parity selection

Next, we describe the interaction between the modes $\mathbf{a_s}$ and $\mathbf{a_{r_2}}$. We propose to engineer a beam-splitter-like interaction of the form $\mathbf{a_s}\mathbf{a_{r_2}}^\dagger + \mathbf{a_s}^\dagger\mathbf{a_{r_2}}$ *conditioned on the number of photons in the* $\mathbf{a_s}$ *mode being* $2\tilde{n}+1$. This interaction has the effect that when the mode $\mathbf{a_s}$ has $2\tilde{n}+1$ photons, a photon of the $\mathbf{a_s}$ mode is destroyed, in turn creating a photon in the mode $\mathbf{a_{r_2}}$, which is rapidly and irreversibly lost to the environment due to its low-Q nature of resonator r_2. This state-selective beam-splitter interaction is generated by a stiff pump incident on the readout cavity r_2 at frequency $\omega_{p'} = (\omega_{r_2} - \omega_s - 2\tilde{n}\chi_{sr_2})/2$ (see below for more details). To realize the number selectivity of this interaction, we need to work in the strong dispersive regime of the storage cavity. This ensures that the beam-splitter interaction becomes off resonant when the number of photons in mode $\mathbf{a_s}$ is anything but $2\tilde{n}+1$. The Hamiltonian describing the interaction between modes $\mathbf{a_s}$ and $\mathbf{a_{r_2}}$ is given by (see Fig. 4)

$$\mathbf{H}_{sr_2} = \omega_s \mathbf{a_s}^\dagger \mathbf{a_s} + \omega_{r_1}\mathbf{a_{r_2}}^\dagger \mathbf{a_{r_2}} + g_{\text{ps}}\left(e^{2i\omega_{p'}t}\mathbf{a_s}^\dagger \mathbf{a_{r_2}} + e^{-2i\omega_{p'}t}\mathbf{a_s}\mathbf{a_{r_2}}^\dagger\right) - \frac{\chi_{ss}}{2}\mathbf{a_s}^{\dagger 2}\mathbf{a_s}^2 - \frac{\chi_{r_2 r_2}}{2}\mathbf{a_{r_2}}^{\dagger 2}\mathbf{a_{r_2}}^2 - \chi_{sr_2}(\mathbf{a_s}^\dagger\mathbf{a_s})\left(\mathbf{a_{r_2}}^\dagger\mathbf{a_{r_2}}\right), \quad (9)$$

where g_{ps} is the strength of the beam-splitter interaction fixed by the pump amplitude ($\epsilon_{p'}$) and is given by

$$g_{\text{ps}} = \sqrt{\chi_{r_2 r_2}\chi_{sr_2}}\left|\frac{\epsilon_{p'}}{\omega_{p'} - \omega_{r_2}}\right|^2. \quad (10)$$

Due to the rate inequalities of Eq. (6), it suffices to keep only the cross-Kerr interaction $-\chi_{sr_2}(\mathbf{a_s}^\dagger\mathbf{a_s})(\mathbf{a_{r_2}}^\dagger\mathbf{a_{r_2}})$ for the calculation. The selectivity of the transition between the levels

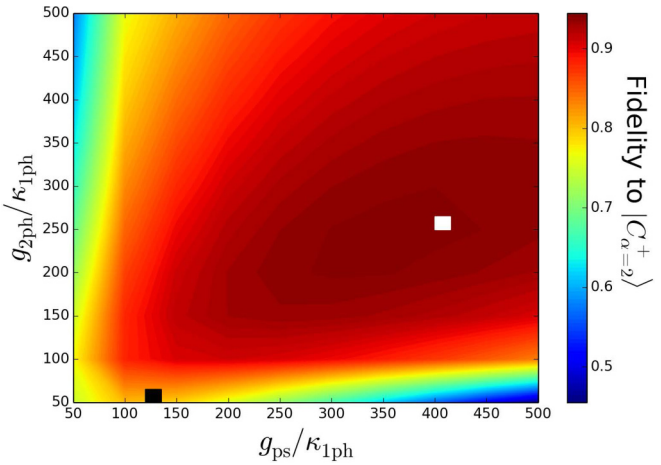

FIG. 5. (Color online) Fidelity with respect to the target cat state, obtained by solving Eq. (11), vs parameters $g_{2\mathrm{ph}}/\kappa_{1\mathrm{ph}}, g_{\mathrm{ps}}/\kappa_{1\mathrm{ph}}$. We choose $\kappa_{r_1} = \kappa_{r_2} = 10^3\kappa_{1\mathrm{ph}}, \chi_{sr_2} = 2.5 \times 10^4\kappa_{1\mathrm{ph}}$. The ratio of ϵ_{r_1} and $g_{2\mathrm{ph}}$ is chosen to be 4 so that the target cat state is $|C^{+}_{\alpha=2}\rangle$. The white square denotes the point of optimal fidelity, $\simeq$0.94 for this choice of parameters ($g_{2\mathrm{ph}} = 250\kappa_{1\mathrm{ph}}, g_{\mathrm{ps}} = 400\kappa_{1\mathrm{ph}}$; cf. Fig. 2). The black square is the point in the shown range of parameters where the adiabatic elimination of Sec. III C works best.

$|2\tilde{n}+1\rangle_{a_s} \otimes |0\rangle_{a_{r_2}}$ and $|2\tilde{n}\rangle_{a_s} \otimes |1\rangle_{a_{r_2}}$ is ensured by detuning the frequency of the stiff pump ($\omega_{p'}$) from $(\omega_{r_2} - \omega_s)/2$ by $-\tilde{n}\chi_{sr_2}$.[3] This leads to strong number selectivity when $\chi_{sr_2} \gg g_{\mathrm{ps}}$. In addition, the cross-Kerr interaction also has to be stronger than the damping of the low-Q mode $\mathbf{a_{r_2}}$, i.e., $\chi_{sr_2} \gg \kappa_{r_2}$ so that the state selectivity is not washed away by dissipation-induced level broadening.

Moving to the rotating frame $\mathbf{a_s} \to \mathbf{a_s}e^{-i\omega_s t}, \mathbf{a_{r_1}} \to \mathbf{a_{r_1}}e^{-i\omega_{r_1}t}, \mathbf{a_{r_2}} \to \mathbf{a_{r_2}}e^{-i\omega_{r_2}t+2i\tilde{n}\chi_{sr_2}t}$, we can now write the master equation for the density matrix ($\rho_{sr_1r_2}$) for the full three-mode model associated with $\mathbf{a_s}, \mathbf{a_{r_1}}$, and $\mathbf{a_{r_2}}$:

$$\frac{d\rho_{sr_1r_2}}{dt} = -i\left[\bar{\mathbf{H}}_{2\mathrm{ph}} + \mathbf{H}_{\mathrm{ps}} + \mathbf{H}_{\mathrm{cross-Kerr}}, \rho_{sr_1r_2}\right] + \left[\kappa_{r_1}\mathcal{D}(\mathbf{a_{r_1}}) + \kappa_{r_2}\mathcal{D}(\mathbf{a_{r_2}}) + \kappa_{1\mathrm{ph}}\mathcal{D}(\mathbf{a_s})\right]\rho_{sr_1r_2}, \quad (11)$$

where

$$\begin{aligned} \bar{\mathbf{H}}_{2\mathrm{ph}} &= g_{2\mathrm{ph}}\left(\mathbf{a_s}^{\dagger 2}\mathbf{a_{r_1}} + \mathbf{a_s}^2\mathbf{a_{r_1}}^\dagger\right) - \epsilon_{r_1}\left(\mathbf{a_{r_1}} + \mathbf{a_{r_1}}^\dagger\right), \\ \mathbf{H}_{\mathrm{ps}} &= g_{\mathrm{ps}}\left(\mathbf{a_s}\mathbf{a_{r_2}}^\dagger + \mathbf{a_s}^\dagger\mathbf{a_{r_2}}\right), \\ \mathbf{H}_{\mathrm{cross-Kerr}} &= \chi_{sr_2}(2\tilde{n} - \mathbf{a_s}^\dagger\mathbf{a_s})\mathbf{a_{r_2}}^\dagger\mathbf{a_{r_2}}. \end{aligned} \quad (12)$$

We now present the numerical results obtained from numerically solving the above three-mode master equation. In Fig. 5, we plot the fidelity with respect to the target cat state ($|C^{+}_{\alpha=2}\rangle$) upon variation of the parameters $g_{2\mathrm{ph}}/\kappa_{1\mathrm{ph}}$ and $g_{\mathrm{ps}}/\kappa_{1\mathrm{ph}}$. The choice of parameters is as follows: $\kappa_{r_1} = \kappa_{r_2} = 10^3\kappa_{1\mathrm{ph}}, \chi_{r_1s} = 2.5 \times 10^4\kappa_{1\mathrm{ph}}$. The ratio $\epsilon_{r_1}/g_{2\mathrm{ph}} = 4$, so that the target cat state is $|C^{+}_{\alpha=2}\rangle$. We see that for this choice of parameters, the optimal fidelity ($\sim$0.94) is obtained for $g_{2\mathrm{ph}} = 250\kappa_{1\mathrm{ph}}, g_{\mathrm{ps}} = 400\kappa_{1\mathrm{ph}}$. The robustness of the scheme is indicated by the fact that for a large range of parameters, we find fidelities in excess of 90%. Note that $g_{2\mathrm{ph}}$ cannot be increased arbitrarily; due to the inequalities (6) and (8), $g_{2\mathrm{ph}} \leqslant \kappa_{r_1}$. g_{ps} also is bounded, by $\sqrt{\chi_{r_2r_2}\chi_{sr_2}}$ [cf. Eq. (10)], which is much larger than κ_{r_2}. For both of these variables, these bounds are not reached in our simulations. Noting that the optimal fidelity of $\sim$94% is mainly limited by single-photon loss, a higher-Q storage cavity, while the other parameters are fixed, would improve the target fidelity. Another possibility to achieve high-fidelity cat states is to monitor and condition the generation, on the output of the readout mode r_2: by selecting the events where the output of the r_2 mode is in vacuum for a time duration of order $\kappa_{\mathrm{ps}}^{-1}$, one can significantly increase the cat state fidelity. This selection excludes the events where a single-photon jump has happened but has not yet been corrected.

In the following section, we will show how the above three-mode master equation [Eq. (11)] can be reduced to the single-mode effective master equation [Eq. (3)], with the two-photon dissipation and parity-selection rates given by Eqs. (13) and (26).

C. Elimination of fast dynamics

Due to the low-Q nature of the modes $\mathbf{a_{r_1}}$ and $\mathbf{a_{r_2}}$, we can eliminate their dynamics adiabatically to arrive at a reduced equation of motion for mode $\mathbf{a_s}$. Elimination of the $\mathbf{a_{r_1}}$ mode can be done following chapter 12 of [43]. This gives rise to a two-photon dissipation rate,

$$\kappa_{2\mathrm{ph}} = \frac{4g_{2\mathrm{ph}}^2}{\kappa_{r_1}}. \quad (13)$$

After eliminating the mode $\mathbf{a_{r_1}}$, we proceed to eliminate the fast dynamics associated with the mode $\mathbf{a_{r_2}}$. In the rotating frame of the Hamiltonian $\mathbf{H}_{\mathrm{cross-Kerr}}$, the reduced master equation for the density matrix (ρ_{sr_2}) for the modes $\mathbf{a_s}, \mathbf{a_{r_2}}$ is given by

$$\frac{d\rho_{sr_2}}{dt} = -i\left[i\left(\epsilon_{2\mathrm{ph}}\mathbf{a_s}^{\dagger 2} - \epsilon_{2\mathrm{ph}}^*\mathbf{a_s}^2\right)\Pi_{|0\rangle_{a_{r_2}}}, \rho_{sr_2}\right] + \kappa_{2\mathrm{ph}}\mathcal{D}\left(\mathbf{a_s}^2\Pi_{|0\rangle_{a_{r_2}}}\right)\rho_{sr_2} + \mathcal{L}_{sr_2}\rho_{sr_2}, \quad (14)$$

where

$$\begin{aligned} \mathcal{L}_{sr_2}\rho_{sr_2} = -ig_{\mathrm{ps}}\sum_{j=0}^{\infty}\Big\{&\left[\Pi_{|2\tilde{n}+1-j\rangle_{a_s}\otimes|j\rangle_{a_{r_2}}}\mathbf{a_s}^\dagger\mathbf{a_{r_2}} + \mathbf{a_s}\mathbf{a_{r_2}}^\dagger\Pi_{|2\tilde{n}+1-j\rangle_{a_s}\otimes|j\rangle_{a_{r_2}}}, \rho_{sr_2}\right] \\ &+ \kappa_{r_2}\mathcal{D}\left(\mathbf{a_{r_2}}\Pi_{|j\rangle_{a_s}}\right)\rho_{sr_2} + \kappa_{1\mathrm{ph}}\mathcal{D}\left(\mathbf{a_s}\Pi_{|j\rangle_{a_{r_2}}}\right)\rho_{sr_2}\Big\}, \end{aligned} \quad (15)$$

and $\Pi_{|0\rangle_{a_{r_2}}} = |0\rangle_{a_{r_2}a_{r_2}}\langle 0|, \Pi_{|2\tilde{n}+1-j\rangle_{a_s}\otimes|j\rangle_{a_{r_2}}} = |2\tilde{n}+1-j\rangle_{a_s} \otimes |j\rangle_{a_{r_2}a_{r_2}}\langle j| \otimes {}_{a_s}\langle 2\tilde{n}+1-j|$. In writing Eqs. (14) and (15), we have made use of the rotating wave approximation, assuming that $\chi_{sr_2} \gg \kappa_{r_2}, g_{\mathrm{ps}}$. In principle, for $\kappa_{r_2} > g_{\mathrm{ps}}$, we can adiabatically eliminate the dynamics of the low-Q mode $\mathbf{a_{r_2}}$. However, a direct calculation from Eqs. (14) and (15) is difficult since any level of the mode $\mathbf{a_{r_2}}$ can be excited. Instead, we approximately calculate an effective rate of transition

[3] In the case of stabilizing an odd cat state, $\omega_{p'}$ is detuned from $(\omega_{r_2} - \omega_s)/2$ by $-(\tilde{n} + 1/2)\chi_{sr_2}$, where $2\tilde{n}+1$ is the odd integer closest to the average number of photons in the target cat state.

of the system from the state $|2\tilde{n}+1\rangle_{a_s}\otimes|0\rangle_{a_{r_2}}$ to the state $|2\tilde{n}\rangle_{a_s}\otimes|0\rangle_{a_{r_2}}$ via the state $|2\tilde{n}\rangle_{a_s}\otimes|1\rangle_{a_{r_2}}$. Note that since the $\mathbf{a_{r_2}}$ mode is low Q and there is no drive resonant at ω_{r_2}, $\mathbf{a_{r_2}}$ gets populated solely due to the interaction term of the form $\mathbf{a_s a_{r_2}}^\dagger$ in Eq. (15). Hence we can expand the two-mode density matrix ρ_{sr_2} as

$$\begin{aligned}\rho_{sr_2} &= \rho_{00}|0\rangle_{a_{r_2}a_{r_2}}\langle 0| + \delta\big(\rho_{01}|0\rangle_{a_{r_2}a_{r_2}}\langle 1| + \rho_{10}|1\rangle_{a_{r_2}a_{r_2}}\langle 0|\big)\\ &\quad + \delta^2\big(\rho_{11}|1\rangle_{a_{r_2}a_{r_2}}\langle 1| + \rho_{20}|2\rangle_{a_{r_2}a_{r_2}}\langle 0| + \rho_{02}|0\rangle_{a_{r_2}a_{r_2}}\langle 2|\big)\\ &\quad + O(\delta^3),\end{aligned} \tag{16}$$

where $\rho_{ij}, i,j=0,1,2$ act on the Hilbert space of the $\mathbf{a_s}$ mode. The natural small parameter of expansion is $\delta = g_{\rm ps}/\kappa_{r_2}$ (for similar analysis, cf. [44]). We will show that the short-lived states ρ_{01},ρ_{10}, and ρ_{11} can be adiabatically eliminated in favor of an effective dynamics of ρ_{00}. We will also see that ρ_{20},ρ_{02} can be dropped for a reduced dynamics in the sector of Hilbert space of $\mathbf{a_s}$ which is of interest to us: span of $\{|2\tilde{n}\rangle_{a_s},|2\tilde{n}+1\rangle_{a_s}\}$. For this calculation, we omit the two-photon drive and/or dissipation which acts only on ρ_{00} and the single-photon loss, the rate of which is much slower than the fast time scale of the adiabatic elimination. These terms gives rise to a correction only in orders of $O(\kappa_{1\rm ph}/\kappa_{r_2})$ and can be neglected. We will reinsert them at the end to get the final evolution of the reduced density matrix of mode $\mathbf{a_s}$. Thus, from Eqs. (14) and (15), we can write down an equation of motion for $\rho_{ij}, i,j=0,1,2$ in dimensionless variable $\tau=\kappa_{r_2}t$:

$$\begin{aligned}\frac{d\rho_{00}}{d\tau} &= -i\delta^2\big(\Pi_{|2\tilde{n}+1\rangle_{a_s}}\mathbf{a_s}^\dagger\rho_{10} - \rho_{01}\mathbf{a_s}\Pi_{|2\tilde{n}+1\rangle_{a_s}}\big)\\ &\quad + \delta^2\sum_{n=0}^{\infty}\Pi_{|n\rangle_{a_s}}\rho_{11}\Pi_{|n\rangle_{a_s}},\\ \frac{d\rho_{11}}{d\tau} &= -i\big(\mathbf{a_s}\Pi_{|2\tilde{n}+1\rangle_{a_s}}\rho_{01} - \rho_{10}\Pi_{|2\tilde{n}+1\rangle_{a_s}}\mathbf{a_s}^\dagger\big) - \rho_{11},\\ \frac{d\rho_{01}}{d\tau} &= -i\big(\delta^2\Pi_{|2\tilde{n}+1\rangle_{a_s}}\mathbf{a_s}^\dagger\rho_{11} - \rho_{00}\Pi_{|2\tilde{n}+1\rangle_{a_s}}\mathbf{a_s}^\dagger\\ &\quad - \sqrt{2}\delta^2\rho_{02}\mathbf{a_s}\Pi_{|2\tilde{n}+2\rangle_{a_s}}\big) - \frac{1}{2}\rho_{01},\\ \frac{d\rho_{10}}{d\tau} &= -i\big(\mathbf{a_s}\Pi_{|2\tilde{n}+1\rangle_{a_s}}\rho_{00} + \sqrt{2}\delta^2\Pi_{|2\tilde{n}+2\rangle_{a_s}}\mathbf{a_s}^\dagger\rho_{20}\\ &\quad - \delta^2\rho_{11}\mathbf{a_s}\Pi_{|2\tilde{n}+1\rangle_{a_s}}\big) - \frac{1}{2}\rho_{10},\\ \frac{d\rho_{20}}{d\tau} &= -i\sqrt{2}\mathbf{a_s}\Pi_{|2\tilde{n}+2\rangle_{a_s}}\rho_{10} - \rho_{20},\\ \frac{d\rho_{02}}{d\tau} &= i\sqrt{2}\rho_{01}\Pi_{|2\tilde{n}+2\rangle_{a_s}}\mathbf{a_s}^\dagger - \rho_{02}.\end{aligned} \tag{17}$$

Define

$$\begin{aligned}&\rho_{ij}^m = {}_{a_s}\langle m|\rho_{ij}|m\rangle_{a_s},\ \ i,j=0,1,\ \ m=2\tilde{n},2\tilde{n}+1,\\ &\bar{\rho}_{ij} = {}_{a_s}\langle 2\tilde{n}|\rho_{ij}|2\tilde{n}+1\rangle_{a_s},\quad \bar{\bar{\rho}}_{ij} = {}_{a_s}\langle 2\tilde{n}+1|\rho_{ij}|2\tilde{n}\rangle_{a_s}.\end{aligned} \tag{18}$$

Then, from Eq. (17), we can write

$$\begin{aligned}\frac{d\rho_{00}^{2\tilde{n}+1}}{d\tau} &= -i\delta^2\sqrt{2\tilde{n}+1}(\bar{\rho}_{10}-\bar{\bar{\rho}}_{01}) + \delta^2\rho_{11}^{2\tilde{n}+1},\\ \frac{d\rho_{11}^{2\tilde{n}+1}}{d\tau} &= -\rho_{11}^{2\tilde{n}+1},\\ \frac{d\rho_{01}^{2\tilde{n}+1}}{d\tau} &= -i\delta^2\sqrt{2\tilde{n}+1}\bar{\rho}_{11} - \frac{1}{2}\rho_{01}^{2\tilde{n}+1},\\ \frac{d\rho_{10}^{2\tilde{n}+1}}{d\tau} &= i\delta^2\sqrt{2\tilde{n}+1}\bar{\bar{\rho}}_{11} - \frac{1}{2}\rho_{10}^{2\tilde{n}+1}.\end{aligned} \tag{19}$$

We see that the dynamics of $\rho_{11}^{2\tilde{n}+1},\rho_{01}^{2\tilde{n}+1}$, and $\rho_{10}^{2\tilde{n}+1}$ occur on a much faster time scale than $\rho_{00}^{2\tilde{n}+1}$ and thus, while performing adiabatic elimination, we can replace them by their steady-state values:

$$\begin{aligned}&\big[\rho_{11}^{2\tilde{n}+1}\big]_{\rm s.s.} = 0,\quad \big[\rho_{01}^{2\tilde{n}+1}\big]_{\rm s.s.} = -2i\delta^2\sqrt{2\tilde{n}+1}\big[\bar{\rho}_{11}\big]_{\rm s.s.},\\ &\big[\rho_{10}^{2\tilde{n}+1}\big]_{\rm s.s.} = 2i\delta^2\sqrt{2\tilde{n}+1}[\bar{\bar{\rho}}_{11}]_{\rm s.s.}.\end{aligned} \tag{20}$$

Similarly, we can write down the equation of motion for $\rho_{ij}^{2\tilde{n}}$:

$$\begin{aligned}\frac{d\rho_{00}^{2\tilde{n}}}{d\tau} &= \delta^2\rho_{11}^{2\tilde{n}},\\ \frac{d\rho_{11}^{2\tilde{n}}}{d\tau} &= i\sqrt{2\tilde{n}+1}(\bar{\rho}_{10}-\bar{\bar{\rho}}_{01}) - \rho_{11}^{2\tilde{n}},\\ \frac{d\rho_{01}^{2\tilde{n}}}{d\tau} &= i\sqrt{2\tilde{n}+1}\bar{\rho}_{00} - \frac{1}{2}\rho_{01}^{2\tilde{n}},\\ \frac{d\rho_{10}^{2\tilde{n}}}{d\tau} &= -i\sqrt{2\tilde{n}+1}\bar{\bar{\rho}}_{00} - \frac{1}{2}\rho_{10}^{2\tilde{n}},\end{aligned} \tag{21}$$

the steady-state solutions of which give us

$$\begin{aligned}\big[\rho_{11}^{2\tilde{n}}\big]_{\rm s.s.} &= -i\sqrt{2\tilde{n}+1}([\bar{\bar{\rho}}_{01}]_{\rm s.s.} - [\bar{\rho}_{10}]_{\rm s.s.}),\\ \big[\rho_{01}^{2\tilde{n}}\big]_{\rm s.s.} &= 2i\sqrt{2\tilde{n}+1}\big[\bar{\rho}_{00}\big]_{\rm s.s.},\\ \big[\rho_{10}^{2\tilde{n}}\big]_{\rm s.s.} &= -2i\sqrt{2\tilde{n}+1}\big[\bar{\bar{\rho}}_{00}\big]_{\rm s.s.}.\end{aligned} \tag{22}$$

Using Eqs. (19)–(22), we can write down equations of motion for $\rho_{00}^{2\tilde{n}}$ and $\rho_{00}^{2\tilde{n}+1}$:

$$\begin{aligned}\frac{d\rho_{00}^{2\tilde{n}+1}}{d\tau} &= -i\delta^2\sqrt{2\tilde{n}+1}([\bar{\rho}_{10}]_{\rm s.s.} - [\bar{\bar{\rho}}_{01}]_{\rm s.s.}),\\ \frac{d\rho_{00}^{2\tilde{n}}}{d\tau} &= i\delta^2\sqrt{2\tilde{n}+1}([\bar{\rho}_{10}]_{\rm s.s.} - [\bar{\bar{\rho}}_{01}]_{\rm s.s.}).\end{aligned} \tag{23}$$

Note that $\frac{d\rho_{00}^{2\tilde{n}+1}}{d\tau} + \frac{d\rho_{00}^{2\tilde{n}}}{d\tau} = 0$, which signifies that the population of the state $|2\tilde{n}+1\rangle_{a_s}\otimes|0\rangle_{a_{r_2}}$, does indeed decay to $|2\tilde{n}\rangle_{a_s}\otimes|0\rangle_{a_{r_2}}$. To complete the analysis and get an explicit form of the rate of population transfer, we write down the equation of motion for $\bar{\rho}_{10},\bar{\bar{\rho}}_{01}$:

$$\begin{aligned}\frac{d\bar{\rho}_{10}}{d\tau} &= -i\sqrt{2\tilde{n}+1}\big(\rho_{00}^{2\tilde{n}+1} - \delta^2\rho_{11}^{2\tilde{n}}\big) - \frac{1}{2}\bar{\rho}_{10},\\ \frac{d\bar{\bar{\rho}}_{01}}{d\tau} &= i\sqrt{2\tilde{n}+1}\big(\rho_{00}^{2\tilde{n}+1} - \delta^2\rho_{11}^{2\tilde{n}}\big) - \frac{1}{2}\bar{\bar{\rho}}_{01},\end{aligned}$$

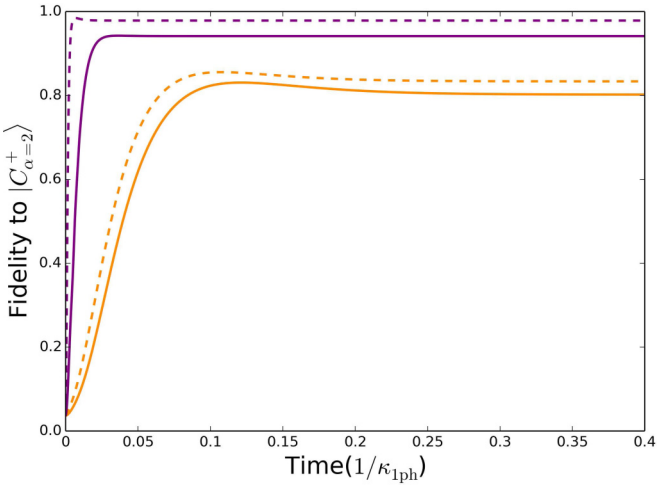

FIG. 6. (Color online) Comparison between the evolution of fidelities for the full three-mode master equation [Eq. (11)] in solid lines, and that obtained from the reduced dynamics [Eqs. (3) and (26)] in dashed lines. The two sets of parameters are chosen from Fig. 5: the white square (purple curves) corresponding to $g_{\mathrm{ps}} = 400\kappa_{1\mathrm{ph}}, g_{2\mathrm{ph}} = 250\kappa_{1\mathrm{ph}}$, and $\epsilon_{r_1} = 1000\kappa_{1\mathrm{ph}}$, and the black square (orange curves) corresponding to $g_{\mathrm{ps}} = 120\kappa_{1\mathrm{ph}}, g_{2\mathrm{ph}} = 50\kappa_{1\mathrm{ph}}$, and $\epsilon_{r_1} = 200\kappa_{1\mathrm{ph}}$. For both sets of curves, $\chi_{sr_2} = 2.5 \times 10^4\kappa_{1\mathrm{ph}}, \kappa_{r_2} = \kappa_{r_1} = 1000\kappa_{1\mathrm{ph}}$ and the target state is $|C^+_{\alpha=2}\rangle$. The model reduction [Eq. (3)] approaches the full three-mode master equation [Eq. (11)] as the adiabatic approximation $(g_{2\mathrm{ph}}/\kappa_{r_1} \ll 1, g_{\mathrm{ps}}/\kappa_{r_2} \ll 1)$ and the rotating wave approximation $(g_{\mathrm{ps}}/\chi_{sr_2} \ll 1, \kappa_{r_2}/\chi_{sr_2} \ll 1)$ become more and more accurate.

the steady-state solutions of which are

$$[\bar{\rho}_{10}]_{\mathrm{s.s.}} = -[\bar{\bar{\rho}}_{01}]_{\mathrm{s.s.}} = -2i\sqrt{2\tilde{n}+1}\left(\rho_{00}^{2\tilde{n}+1} - \delta^2\rho_{11}^{2\tilde{n}}\right). \quad (24)$$

Using Eqs. (22)–(24) and some tedious algebra, we have (in dimensional variables)

$$\frac{d\rho_{00}^{2\tilde{n}+1}}{dt} = -\kappa_{\mathrm{ps}}\rho_{00}^{2\tilde{n}+1}, \qquad \frac{d\rho_{00}^{2\tilde{n}}}{dt} = \kappa_{\mathrm{ps}}\rho_{00}^{2\tilde{n}+1}, \quad (25)$$

where

$$\kappa_{\mathrm{ps}} = \frac{4\delta^2(2\tilde{n}+1)}{1+4\delta^2(2\tilde{n}+1)}\kappa_{r_2}. \quad (26)$$

Thus we have indeed derived an effective dynamics for the reduced density matrix of the storage mode: $\rho = \mathrm{Tr}_{a_{r_2}}[\rho_{sr_2}]$ as given by Eq. (3) of Sec. II with κ_{ps} given by Eq. (26).

The key requirements for the above model reduction are the validity of the adiabatic approximation $(g_{2\mathrm{ph}}/\kappa_{r_1} \ll 1, g_{\mathrm{ps}}/\kappa_{r_2} \ll 1)$ and the rotating wave approximation $(g_{\mathrm{ps}}/\chi_{sr_2} \ll 1, \kappa_{r_2}/\chi_{sr_2} \ll 1)$. In Fig. 6, we compare the validity of the model reduction for two choice of parameters (cf. Fig. 5): the white square (purple curves) corresponding to $g_{\mathrm{ps}} = 400\kappa_{1\mathrm{ph}}, g_{2\mathrm{ph}} = 250\kappa_{1\mathrm{ph}}$, and $\epsilon_{r_1} = 1000\kappa_{1\mathrm{ph}}$, and the black square (orange curves) corresponding to $g_{\mathrm{ps}} = 120\kappa_{1\mathrm{ph}}, g_{2\mathrm{ph}} = 50\kappa_{1\mathrm{ph}}$, and $\epsilon_{r_1} = 200\kappa_{1\mathrm{ph}}$. For both sets of curves, $\chi_{sr_2} = 2.5 \times 10^4\kappa_{1\mathrm{ph}}, \kappa_{r_2} = \kappa_{r_1} = 1000\kappa_{1\mathrm{ph}}$ and the target state is $|C^+_{\alpha=2}\rangle$. The model reduction [Eq. (3)] approaches the full three-mode master equation [Eq. (11)] as the adiabatic approximation $(g_{2\mathrm{ph}}/\kappa_{r_1} \ll 1, g_{\mathrm{ps}}/\kappa_{r_2} \ll 1)$ and the rotating wave approximation $(g_{\mathrm{ps}}/\chi_{sr_2} \ll 1, \kappa_{r_2}/\chi_{sr_2} \ll 1)$ becomes more and more accurate.

IV. CONCLUSIONS

Following recent advances in the production of nonclassical states of light, we have proposed a scheme to prepare, and protect against decoherence, Schrödinger cat states of given photon-number parity. Relying only on the application of continuous-wave drives of fixed but carefully chosen frequencies, we are able to engineer an effective Hamiltonian and dissipation which stabilizes such states. The scheme is independent of the phase of the drives and appears to be robust with respect to the choice of their amplitudes. Numerical simulations illustrate that the required parameters are within reach of the ongoing experiments in the field of quantum superconducting circuits. Such a stabilized source of Schrödinger cat states is a valuable system component that could be integrated in existing quantum information processing schemes based only on linear optical scattering elements and amplifiers.

ACKNOWLEDGMENTS

Discussions with Pierre Rouchon and Benjamin Huard are gratefully acknowledged. The work was supported by NSF Grant No. ECCS 1068642 and US Army Research Office Grant No. W911NF-09-1-0514. A.R. and M.M. acknowledge the support of Idex ANR-10-IDEX-0001-02 PSL*.

[1] D. Deutsch, Proc. R. Soc. London **400**, 97 (1985).
[2] R. P. Feynman, Opt. News **11**, 11 (1985).
[3] P. Shor, in *Proceedings of the 35nd Annual Symposium on Foundations of Computer Science*, edited by Shafi Goldwasser (IEEE Computer Society Press, Washington, D.C., 1994), p. 124.
[4] D. P. DiVincenzo, Science **270**, 255 (1995).
[5] S. D. Bartlett, B. C. Sanders, S. L. Braunstein, and K. Nemoto, Phys. Rev. Lett. **88**, 097904 (2002).
[6] J. Eisert, S. Scheel, and M. B. Plenio, Phys. Rev. Lett. **89**, 137903 (2002).
[7] J. Fiurášek, Phys. Rev. Lett. **89**, 137904 (2002).
[8] G. Giedke and J. I. Cirac, Phys. Rev. A **66**, 032316 (2002).
[9] A. Mari and J. Eisert, Phys. Rev. Lett. **109**, 230503 (2012).
[10] B. Yurke and D. Stoler, Phys. Rev. Lett. **57**, 13 (1986).
[11] S. Lloyd and S. L. Braunstein, Phys. Rev. Lett. **82**, 1784 (1999).
[12] E. Knill, R. Laflamme, and G. J. Milburn, Nature (London) **409**, 46 (2001).
[13] H. Jeong and M. S. Kim, Phys. Rev. A **65**, 042305 (2002).
[14] T. C. Ralph, W. J. Munro, and G. J. Milburn, Proc. SPIE **4917**, 1 (2002).
[15] P. Kok, W. J. Munro, K. Nemoto, T. C. Ralph, J. P. Dowling, and G. J. Milburn, Rev. Mod. Phys. **79**, 135 (2007).
[16] A. I. Lvovsky, H. Hansen, T. Aichele, O. Benson, J. Mlynek, and S. Schiller, Phys. Rev. Lett. **87**, 050402 (2001).

[17] S. Fasel, O. Alibart, S. Tanzilli, P. Baldi, A. Beveratos, N. Gisin, and H. Zbinden, New J. Phys. **6**, 163 (2004).
[18] J. S. Neergaard-Nielsen, B. M. Nielsen, H. Takahashi, A. I. Vistnes, and E. S. Polzik, Opt. Express **15**, 7940 (2007).
[19] J.-i. Yoshikawa, K. Makino, S. Kurata, P. van Loock, and A. Furusawa, Phys. Rev. X **3**, 041028 (2013).
[20] E. Bimbard, R. Boddeda, N. Vitrant, A. Grankin, V. Parigi, J. Stanojevic, A. Ourjoumtsev, and P. Grangier, Phys. Rev. Lett. **112**, 033601 (2014).
[21] A. Ourjoumtsev, R. Tualle-Brouri, J. Laurat, and P. Grangier, Science **312**, 83 (2006).
[22] J. S. Neergaard-Nielsen, B. M. Nielsen, C. Hettich, K. Mølmer, and E. S. Polzik, Phys. Rev. Lett. **97**, 083604 (2006).
[23] K. Wakui, H. Takahashi, A. Furusawa, and M. Sasaki, Opt. Express **15**, 3568 (2007).
[24] A. Ourjoumtsev, H. Jeong, R. Tualle-Brouri, and P. Grangier, Nature (London) **448**, 784 (2007).
[25] H. Takahashi, K. Wakui, S. Suzuki, M. Takeoka, K. Hayasaka, A. Furusawa, and M. Sasaki, Phys. Rev. Lett. **101**, 233605 (2008).
[26] S. Deléglise, I. Dotsenko, C. Sayrin, J. Bernu, M. Brune, J.-M. Raimond, and S. Haroche, Nature (London) **455**, 510 (2008).
[27] B. Vlastakis, G. Kirchmair, Z. Leghtas, S. E. Nigg, L. Frunzio, S. M. Girvin, M. Mirrahimi, M. H. Devoret, and R. J. Schoelkopf, Science **342**, 607 (2013).
[28] J. F. Poyatos, J. I. Cirac, and P. Zoller, Phys. Rev. Lett. **77**, 4728 (1996).
[29] A. Sarlette, J. M. Raimond, M. Brune, and P. Rouchon, Phys. Rev. Lett. **107**, 010402 (2011).
[30] M. Mirrahimi, Z. Leghtas, V. V. Albert, S. Touzard, R. J. Schoelkopf, L. Jiang, and M. H. Devoret, New J. Phys. **16**, 045014 (2014).
[31] Z. Leghtas *et al.* (unpublished).
[32] L. Sun, A. Petrenko, Z. Leghtas, B. Vlastakis, G. Kirchmair, K. M. Sliwa, A. Narla, M. Hatridge, S. Shankar, J. Blumoff, L. Frunzio, M. Mirrahimi, M. H. Devoret, and R. J. Schoelkopf, Nature (London) **511**, 444 (2014).
[33] K. Geerlings, Z. Leghtas, I. M. Pop, S. Shankar, L. Frunzio, R. J. Schoelkopf, M. Mirrahimi, and M. H. Devoret, Phys. Rev. Lett. **110**, 120501 (2013).
[34] S. Shankar, M. Hatridge, Z. Leghtas, K. Sliwa, A. Narla, U. Vool, S. Girvin, L. Frunzio, M. Mirrahimi, and M. H. Devoret, Nature (London) **504**, 419 (2013).
[35] Z. Leghtas, U. Vool, S. Shankar, M. Hatridge, S. M. Girvin, M. H. Devoret, and M. Mirrahimi, Phys. Rev. A **88**, 023849 (2013).
[36] E. Holland, B. Vlastakis, R. Heeres, U. Vool, Z. Leghtas, L. Frunzio, G. Kirchmair, M. Mirrahimi, and R. J. Schoelkopf (unpublished).
[37] D. I. Schuster, A. A. Houck, J. A. Schreier, A. Wallraff, J. M. Gambetta, A. Blais, L. Frunzio, J. Majer, B. Johnson, M. H. Devoret, S. M. Girvin, and R. J. Schoelkopf, Nature (London) **445**, 515 (2007).
[38] M. Wolinsky and H. J. Carmichael, Phys. Rev. Lett. **60**, 1836 (1988).
[39] E. E. Hach, III and C. C. Gerry, Phys. Rev. A **49**, 490 (1994).
[40] L. Gilles, B. M. Garraway, and P. L. Knight, Phys. Rev. A **49**, 2785 (1994).
[41] L. Krippner, W. J. Munro, and M. D. Reid, Phys. Rev. A **50**, 4330 (1994).
[42] S. E. Nigg, H. Paik, B. Vlastakis, G. Kirchmair, S. Shankar, L. Frunzio, M. H. Devoret, R. J. Schoelkopf, and S. M. Girvin, Phys. Rev. Lett. **108**, 240502 (2012).
[43] H. Carmichael, *Statistical Methods in Quantum Optics 2: Non-Classical Fields*, Statistical Methods in Quantum Optics (Springer, Berlin, 2007).
[44] H. M. Wiseman and G. J. Milburn, Phys. Rev. A **47**, 642 (1993).